Quaternary Science Reviews 326 (2024) 108502

Contents lists available at ScienceDirect

Quaternary Science Reviews

journal homepage: www.elsevier.com/locate/quascirev

Atmospheric $\Delta^{14}C$ in the northern and southern hemispheres over the past two millennia: Role of production rate, southern hemisphere westerly winds and ocean circulation changes

Hugues Goosse[a,*], Victor Brovkin[b,c], Katrin J. Meissner[d,e], Laurie Menviel[d,f], Anne Mouchet[g], Raimund Muscheler[h], Andreas Nilsson[h]

[a] Earth and Life Institute, Université catholique de Louvain, Louvain-la-Neuve, Belgium
[b] MPI for Meteorology, Hamburg, Germany
[c] Center for Earth System Research and Sustainability, University of Hamburg, Hamburg, Germany
[d] Climate Change Research Centre, University of New South Wales, Sydney, New South Wales, Australia
[e] Australian Research Council Centre of Excellence for Climate Extremes, University of New South Wales, Sydney, New South Wales, Australia
[f] Australian Centre of Excellence in Antarctic Science, University of New South Wales, Sydney, New South Wales, Australia
[g] Freshwater and OCeanic Science Unit of ReSearch (FOCUS), Université de Liège, Liège, Belgium
[h] Department of Geology Lund University, Lund, Sweden

ARTICLE INFO

Handling editor: A. Voelker

Keywords:
Holocene
Paleoclimate modeling
Global
Southern Ocean
Cosmogenic isotopes
Past millennium
Westerly winds
Ocean circulation

ABSTRACT

The variations of atmospheric $\Delta^{14}C$ over the past two millennia are classically attributed to changes in its production rate in the upper atmosphere, which in turn is related to changes in solar activity and the Earth's magnetic field. However, the potential contribution of atmospheric and oceanic circulation changes during this period has not been precisely quantified. This has been achieved here using a coupled climate model simulating explicitly the evolution of the different carbon isotopes, driven by a new estimate of ^{14}C production derived from ^{10}Be measurements, and using different production rates for each hemisphere. Our results confirm that changes in global and hemispheric atmospheric $\Delta^{14}C$ are primarily driven by changes in production rate. The very good agreement between our results and observed atmospheric $\Delta^{14}C$ also highlights the strong consistency of current interpretations of ^{10}Be and ^{14}C measurements. By contrast, the interhemispheric difference in atmospheric $\Delta^{14}C$ is controlled by changes in the intensity of southern hemisphere westerly winds (SHWW) that impact atmosphere-ocean exchange and the upwelling of ^{14}C depleted water masses in the Southern Ocean. Changes in deep water formation in both hemispheres or open ocean polynyas in the Southern Ocean only have a small impact on atmospheric $\Delta^{14}C$ over that period. When driven by changes in the SHWW proportional to three existing reconstructions of the Southern Annular Mode (SAM) index, the model reproduces some key characteristics of the observed interhemispheric $\Delta^{14}C$ gradient. These include the low values in the 15th century and the peak in the 16th century, but there are also clear differences between the experiments and $\Delta^{14}C$ observations. This suggests that while SAM reconstructions capture some robust features in the centennial variability, large uncertainties remain.

1. Introduction

^{14}C (radiocarbon) is a radioactive isotope of carbon predominantly produced from nitrogen atoms in the upper atmosphere through the action of cosmic rays. It is widely used in paleoclimatology as a dating tool and as a tracer to diagnose exchanges between and within different carbon reservoirs. The analysis of observed changes in ^{14}C and their modelling has thus provided key information on the past variability of the carbon cycle and oceanic circulation (see the recent reviews of Heaton et al., 2021; Skinner and Bard, 2022).

The amount of ^{14}C has been measured in a wide range of archives and is usually expressed by the $\Delta^{14}C$ of the sample, defined as the deviation of $^{14}C/^{12}C$ from a standard, with correction for fractionation and radioactive decay (e.g., Stuiver and Polach, 1977). Syntheses of ^{14}C

* Corresponding author.
E-mail address: hugues.goosse@uclouvain.be (H. Goosse).

https://doi.org/10.1016/j.quascirev.2024.108502
Received 31 October 2023; Received in revised form 2 January 2024; Accepted 3 January 2024
Available online 13 January 2024

measurements performed in archives that are strongly connected to the atmospheric content, such as tree rings, plant macrofossils, speleothems, varved lake sediments, and some marine archives, have led to estimates of atmospheric $\Delta^{14}C$ for each hemisphere over the past 50,000 years, the most recent estimates being IntCal20 (Reimer et al., 2020) and SHCal20 (Hogg et al., 2020).

In the ocean, ^{14}C can be considered to the first order as a passive tracer which is incorporated at the surface and whose amount decreases with time because of its radioactive decay as it is transported in the ocean interior. The ^{14}C amount at depth at any location thus gives an indication of the time elapsed since the water has last been in contact with the surface, and therefore of the ventilation rate, although the link can be complex (Broecker et al., 1991; Deleersnijder et al., 2001; England and Maier-Reimer, 2001; Skinner and Bard, 2022).

Consequently, analyzing spatial and temporal variations in $\Delta^{14}C$ in the ocean provides an indirect measure of the ocean ventilation for current or past conditions and evaluating the ability of models to reproduce the observed $\Delta^{14}C$ patterns is a powerful way to diagnose potential biases in the simulated circulation. For present-day conditions, most studies focused on the mean state of the ocean circulation (Toggweiler et al., 1989; England and Maier-Reimer, 2001; Orr et al., 2017). However, the impact of the variability of the oceanic circulation on the oceanic $\Delta^{14}C$ has also been investigated, indicating that changes in the Atlantic Meridional Overturning Circulation (AMOC) and in Southern Hemisphere Westerly Winds (SHWW) can have a modest but measurable imprint on the radiocarbon in the ocean at interannual to decadal time scales (Galbraith et al., 2011; Pookkandy et al., 2023).

The analyses of radiocarbon distribution in the ocean at the last glacial maximum have indicated that the low value of $\Delta^{14}C$ at depth in many regions of the ocean could be attributed to a lower ventilation rate of oceanic waters (e.g., Broecker et al., 1988; Muscheler et al., 2000; Meissner et al., 2003; Menviel et al., 2017; Skinner et al., 2017; Dinauer et al., 2020). During the deglaciation, the observed fluctuations of the atmospheric $\Delta^{14}C$ have been linked to the variability of the deep water formation in the north Atlantic, with complementary contributions from changes in the SHWW, Southern Ocean mixing and sea ice cover, and possibly permafrost thawing. These $\Delta^{14}C$ variations help constrain the processes that led to the atmospheric CO_2 changes, and illustrate the interest of radiocarbon in documenting the carbon cycle dynamics (Köhler et al., 2005, 2014; Meissner, 2007; Tschumi et al., 2011; Bauska et al., 2016; Ganopolski and Brovkin, 2017; Menviel et al., 2018; Skinner et al., 2023).

Over the past two millennia, changes in ocean circulation have been assumed to play a relatively small role. The observed variations in $\Delta^{14}C$ over that period are generally attributed to changes in the production rate of ^{14}C in the atmosphere (e.g., Muscheler et al., 2007; Roth and Joos, 2013). This production rate is dependent on solar activity, with a more active sun leading to a lower production rate by better protecting the Earth from cosmic rays, and, on longer time scales, on geomagnetic field shielding (e.g., Lal and Peters, 1967; Masarik and Beer, 1999). Consequently, changes in the total solar irradiance over the past millennia have been estimated from ^{14}C production rate, the latter being derived from the reconstructions of atmospheric $\Delta^{14}C$ (e.g., Roth and Joos, 2013; Muscheler et al., 2016; Jungclaus et al., 2017).

However, the influence of oceanic circulation on atmospheric $\Delta^{14}C$ over the past millennia may have been underestimated by models as the simulated magnitude of the centennial variability of the oceanic circulation may be too low compared to reconstructions (Rodgers et al., 2011; Galbraith et al., 2011; Laepple and Huybers, 2014). In particular, models struggle to reproduce reconstructed past changes in the Southern Annual Mode (SAM), which is strongly connected to the strength and position of the SHWW (Abram et al., 2014).

The impact of circulation changes might be easier to detect in the hemispheric $\Delta^{14}C$ gradient than in the global mean $\Delta^{14}C$. The mixing between hemispheres in the troposphere is relatively fast, of the order of 1.5 years (Levin et al., 1987; Geller et al., 1997). However, because of the upwelling of ^{14}C depleted deep and intermediate waters in the Southern Ocean, the preindustrial atmospheric $\Delta^{14}C$ is lower in the southern hemisphere than in the northern hemisphere by about 3–4 ‰ (Levin et al., 1987; Rodgers et al., 2011; Hogg et al., 2020). Any change in the SHWW that would affect the intensity of the upwelling could then have an effect on the observed hemispheric $\Delta^{14}C$ gradient (Rodgers et al., 2011; Capano et al., 2020). For instance, Rodgers et al. (2011) argue that a weakening of the SHWW at the end of the 14th century was responsible for the observed decrease in the interhemispheric gradient of atmospheric $\Delta^{14}C$ at that time.

Our goal here is to further investigate the potential role of changes in oceanic circulation and SHWW on atmospheric $\Delta^{14}C$ and its interhemispheric gradient over the preindustrial common era using simulations performed with an Earth System Model of Intermediate Complexity (EMIC) including a representation of the carbon cycle and explicit simulation of ^{12}C, ^{13}C, and ^{14}C. The interest is twofold. First, we quantify the potential error in ^{14}C production rate reconstructions and the derived solar irradiance when based on the assumption that oceanic circulation variability had no impact on $\Delta^{14}C$. Second, simulating ^{14}C and its interhemispheric gradient can provide indirect information on the changes in atmospheric and oceanic circulations over the past millennia. The model and experimental design are described in section 2. Sensitivity experiments are discussed in section 3 to estimate the potential impact of changes in winds, upwelling and deep-water formation on the evolution of $\Delta^{14}C$. This is required here because the changes in circulation over the past two millennia are much more subtle than the changes that have been simulated in the literature in the context of $\Delta^{14}C$, such as variability during the last glacial period and deglaciation. Those past estimates of the role of the circulation could thus not be used here to quantify the potential contribution of the different processes as much more modest variations are expected for the past two millennia. Simulations covering the past two millennia are then analyzed in section 4 before a discussion and conclusions in section 5.

2. Methodology

a. Description of the model.

LOVECLIM1.3 (Goosse et al., 2010) is an Earth system model of intermediate complexity. The model configuration used here is identical to the one in Goosse et al. (2022), except for ^{14}C which was not activated in this previous study. LOVECLIM results from the coupling of the atmospheric model EcBilt (Opsteegh et al., 1998), the ocean and sea ice model CLIO (Goosse and Fichefet, 1999), the vegetation model VECODE (Brovkin et al., 1997) and the ocean carbon cycle model LOCH (Mouchet and François, 1996). $\delta^{13}C$ and $\Delta^{14}C$ evolution in the atmosphere, ocean and over land is computed by estimating the evolution of the three isotopes of carbon in the different reservoirs and the exchanges between them (Mouchet, 2011; Menviel et al., 2017). The evolution of the carbon isotopes in the atmosphere is managed by LOCH, using a simple one dimensional (latitude) diffusive model and is independent of the atmospheric dynamics simulated by EcBilt. A constant diffusion parameter of $3\ 10^6\ m^2s^{-1}$ is applied in this diffusive model, except at the Equator where a value of $2\ 10^5\ m^2s^{-1}$ is imposed to account for the barrier to interhemispheric exchanges, as for instance done in Levin et al. (1987). The LOVECLIM model has a coarse resolution (5.6° by 5.6° for the atmosphere and land, 3° by 3° in the ocean) and includes simplifications in the atmospheric dynamics to be able to perform long simulations and sensitivity experiments. The simulations presented in this manuscript required several thousand years of integration for the ^{14}C to reach equilibrium in all reservoirs.

b. Description of the experiments

In order to obtain an equilibrium state corresponding to year 1 CE that will be used as initial condition in the subsequent experiments, a

10,000-year simulation is first performed with the model using forcing corresponding to 1 CE, including a prescribed CO_2 concentration of 277 ppm, an atmospheric $\delta^{13}C$ value of −6.4 ‰ and an atmospheric $\Delta^{14}C$ value of −15 ‰. Atmospheric CO_2, ^{13}C and ^{14}C are then computed interactively for another 10,000 years in the experiment Ctrl1CE (Table 1), using a ^{14}C production of 1.54 atoms cm^{-2} s^{-1}. This value leads to minimal drift in atmospheric $\Delta^{14}C$ when the carbon cycle is fully interactive (change of less than 1 ‰ over the 10,000 years of this second simulation). 1.54 atoms cm^{-2} s^{-1} is slightly smaller than recent estimates that give mean values higher than 1.6 atoms cm^{-2} s^{-1} for present-day conditions (Kovaltsov et al., 2012; Poluianov et al., 2016; Herbst et al., 2017). It is also lower than the value used in previous experiments using either the modern period or the Holocene as reference (e.g. Roth and Joos, 2013; Hain et al., 2014). However, the period around 1 CE is characterized by a relatively low atmospheric $\Delta^{14}C$, and a low production rate is thus required to match this value, likely due to stronger geomagnetic shielding (Panovska et al., 2023).

From the equilibrium state obtained in Ctrl1CE, idealized sensitivity experiments are first performed to quantify the potential impact of changes in SHWW and deep ocean circulation on the evolution of the atmospheric $\Delta^{14}C$. In experiment Windstep, the wind stress and wind speed are abruptly increased in the Southern Ocean. This increase equals 25 % for wind stress and 12 % for wind speed at 50°S and decreases to zero in a linear way on a 12° wide band on each side of this peak. The magnitude of this change is similar to a Southern Annular Mode index change of 1 and Windstep thus crudely mimics the effect of a change in SAM, as in Goosse et al. (2022).

LOVECLIM has limited open ocean convection in the Southern Ocean and never forms open ocean polynyas. To quantify their potential influence, large vertical mixing coefficients are imposed in a box located in the Weddell Sea (63°S–69°S/20°W–3°E) in experiment Poly. This results in larger deep-water ventilation and reduced ice concentration in winter in the region. While these higher coefficients are imposed during the whole run in Poly, they are applied for 10 consecutive years every 100 years in experiment Poly10 to emulate the effect of the intermittent formation of polynyas. Finally, 0.1 Sv of freshwater is imposed in the North Atlantic and the Southern Ocean in experiments FreshAtl and FreshSO, respectively. This is likely a much larger perturbation than what was observed during the past two millennia but it provides an upper bound of the potential impact of reduced deep-water formation and reduced vertical mixing in LOVECLIM. The freshwater is applied to the grid points adjacent to the continent in the Southern Ocean and around Greenland in the North Atlantic, following the protocol of the Southern Ocean Freshwater release model experiments Initiative (SOFIA) and the North Atlantic Hosing Model Intercomparison Project (NAHosMIP) respectively (Swart et al., 2023; Jackson et al., 2023).

In a second step, transient forcings (solar, orbital, volcanic, non-CO_2 greenhouse gases, aerosols, land use, anthropogenic CO_2 emissions) are applied for the period 1–2000 CE following the PMIP4 recommendations (Jungclaus et al., 2017). As all the currently available climate model simulations, LOVECLIM is not able to reproduce the low frequency variability of the SAM index inferred from proxy records (e.g. Abram et al. 2014). Consequently, in experiments LM_SAM_Dat2018, LM_SAM_Dal2021, and LM_SAM_Kg2023 additional perturbations of the winds are imposed, following the reconstructions of the SAM index of Dätwyler et al. (2018), Dalaiden et al. (2021), and King et al. (2023), respectively (Fig. 1). For these experiments, we use the same latitudinal perturbation profile as in Windstep and vary the magnitude with the SAM index (Goosse et al., 2022).

The variable ^{14}C production rate (Fig. 2) applied in the experiments covering the past two millennia (Table 1) is based on time series of ^{10}Be from an existing compilation of Greenland and Antarctic ice core records (Muscheler et al., 2016) and adding a new record from the South Pole (Winski et al., 2019; Schaefer, 2022). Based on the discussions in Muscheler et al. (2016), we omit inconsistent data from two ice core records (Camp Century and Dome-C) and then normalize all Greenland

Table 1
List of experiments.

Experiment	Forcings	^{14}C production	Westerlies	Specificity
Ctrl1CE	1 CE	1.54 at. cm^{-2} s^{-1}	No perturbation	$\Delta^{14}C$ is close to -15 ‰
Ctrl1CE0	1 CE	1.58 at. cm^{-2} s^{-1}	No perturbation	$\Delta^{14}C$ is close to 0‰
Windstep	1 CE	1.54 at. cm^{-2} s^{-1}	Step increase of the wind stress year 1	
Poly	1 CE	1.54 at. cm^{-2} s^{-1}	No perturbation	Deep mixing imposed in the Weddell Sea
Poly10	1 CE	1.54 at. cm^{-2} s^{-1}	No perturbation	Deep mixing imposed in the Weddell Sea during 10 years every 100 years
FreshAtl	1 CE	1.54 at. cm^{-2} s^{-}	No perturbation	0.1 Sv added to the North Atlantic
FreshSO	1 CE	1.54 at. cm^{-2} s^{-}	No perturbation	0.1 Sv added to the Southern Ocean
LM_Be10	1–2000 CE	derived from ^{10}Be with the same mean value in each hemisphere	No perturbation	
LM_ProdSH10	1–2000 CE	derived from ^{10}Be with a production 10% higher in the southern hemisphere	No perturbation	
LM_ProdSH20	1–2000 CE	derived from ^{10}Be with a production 20% higher in the southern hemisphere	No perturbation	
LM_SAM_Dat2018	1000–2000 CE	derived from ^{10}Be with the same mean value in each hemisphere	SAM index from Dätwyler et al. (2018)	
LM_SAM_Dal2021	1000–2000 CE	derived from ^{10}Be with the same mean value in each hemisphere	SAM index from Dalaiden et al. (2021)	
LM_SAM_Kg2023	1–2000 CE	derived from ^{10}Be with the same mean value in each hemisphere	SAM index from King et al. (2023)	

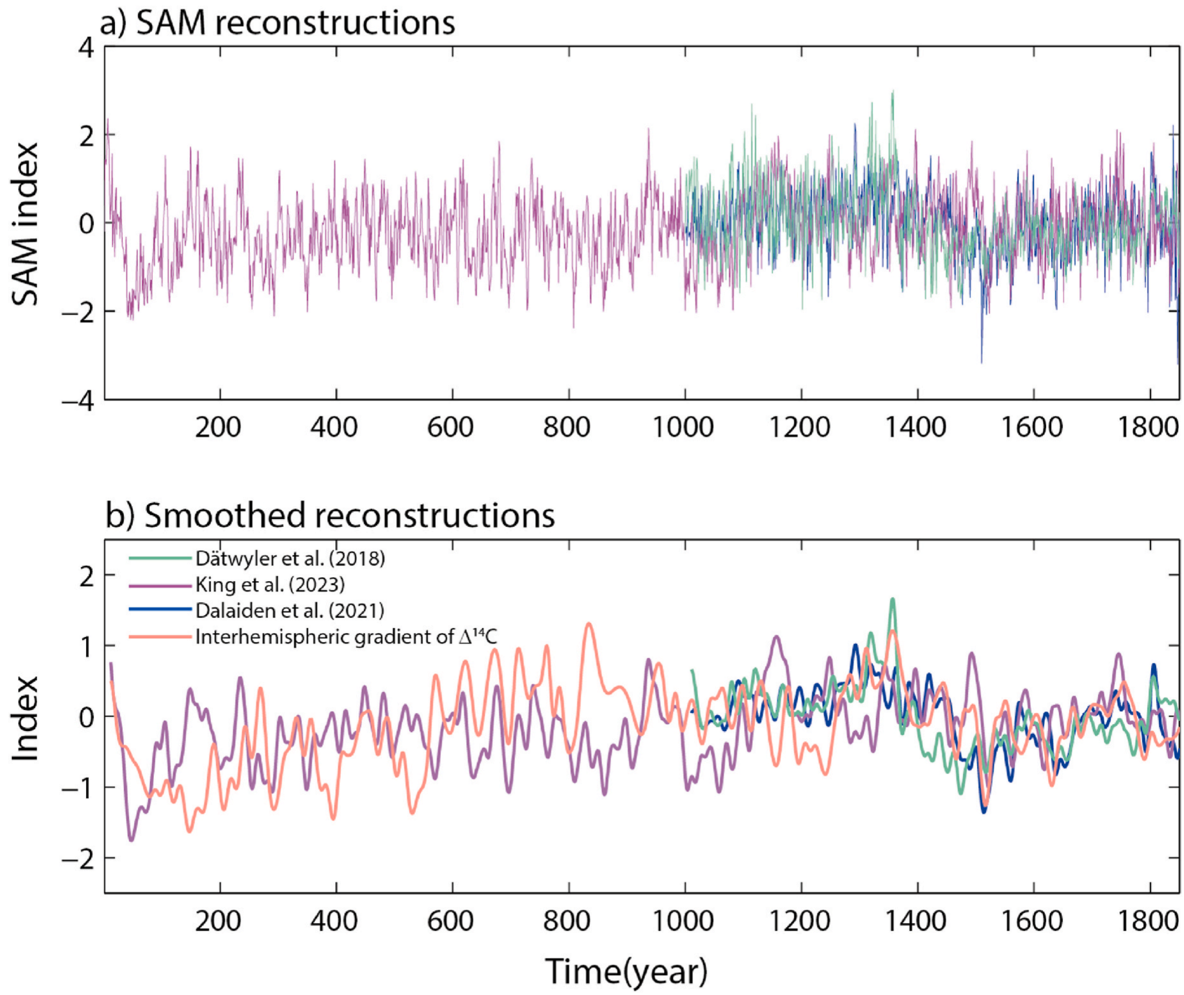

Fig. 1. a) SAM reconstruction time series of Dätwyler et al. (2018) (green), Dalaiden et al. (2021) (blue) and King et al. (2023) (violet) b) same as a) but smoothed using a 21-year hamming filter with, in addition, the interhemispheric gradient of $\Delta^{14}C$ (peach), estimated from the difference between IntCal20 and SHCal20, and scaled to have the same variance as Dätwyler et al. (2018) SAM reconstruction.

records to the NGRIP ^{10}Be data and Antarctic records to the new South pole ^{10}Be data. We assume that the fluctuations in the production of the different cosmogenic isotopes have the same origin and should thus have similar time histories (Bard et al., 1997; Muscheler et al., 2007). This hypothesis has its uncertainties as the production mechanism, the atmospheric transport and the deposition in the archives where it is finally measured, all depend on the isotope (Muscheler et al., 2016; Herbst et al., 2017; Köhler et al., 2022). This leads to uncertainties in the estimate of ^{14}C production rates based on measurement of other cosmogenic isotopes, but it provides series that are completely independent of $\Delta^{14}C$ observations. To investigate the potential impact of hemispherical differences in the production rate, we treat the Greenland and Antarctic ^{10}Be time series separately, assuming that differences between the records are related to differences in production rates (Zheng et al., 2023; Zheng et al., in prep.). For the standard experiment covering the past two millennia (LM_Be10), we multiplied the original data for each hemisphere by a constant that lead to a mean ^{14}C production rate of 1.54 atoms cm^{-2} s^{-1} over the first 1500 years of the experiment and thus match the value selected for the equilibrium control runs. However, recent calculations of cosmogenic radionuclide production rates based on geomagnetic field models over the past 100,000 years suggest higher production rates in the southern hemisphere, with a difference of about 10 % over the past two millennia (Panovska et al., 2023). Consequently, to sample the uncertainty in the hemispheric mean production rate, we have performed two additional sensitivity experiments in which we assume higher production rates on average in the southern hemisphere than in the northern hemisphere: +10% in LM_ProdSH10 and +20% LM_ProdSH20, respectively. This corresponds to mean ^{14}C production rates of 1.46 atoms cm^{-2} s^{-1} in the northern hemisphere and 1.62 atoms cm^{-2} s^{-1} in the southern hemisphere in LM_ProdSH10 and of 1.39 atoms cm^{-2} s^{-1}and 1.69 atoms cm^{-2} s^{-1}in LM_ProdSH20.

c. Evaluation of model performance

LOVECLIM reproduces the differences in $\Delta^{14}C$ between the different water masses relatively well (Fig. 3). If we compare simulated $\Delta^{14}C$ for LM_Be10 averaged over the period 1700–1800 CE with estimates of pre-industrial conditions derived from observations (GLODAP, Key et al., 2004), we see that the model tends to simulate too low values. In the deep ocean, the difference is of the order of 20 ‰, which is of the same order of magnitude as in other model simulations (e.g., Matsumoto et al., 2004; Galbraith et al., 2011; Rodgers et al., 2011; Jahn et al., 2015; Pookkandy et al., 2023). The bias is larger for the Antarctic Intermediate Water in the Atlantic and in the North Pacific around 2000 m depth, where it can reach 30–40 ‰. Part of this underestimation could be due to the relatively low ^{14}C production rate used to obtain the initial condition in LM_Be10 (see section 2b). If we initialize the simulation with another equilibrium experiment (Ctrll1CE0) in which atmospheric $\Delta^{14}C$ is set to 0‰, assuming that this value is closer to the long-term average of atmospheric $\Delta^{14}C$, $\Delta^{14}C$ at depth in the ocean increases by

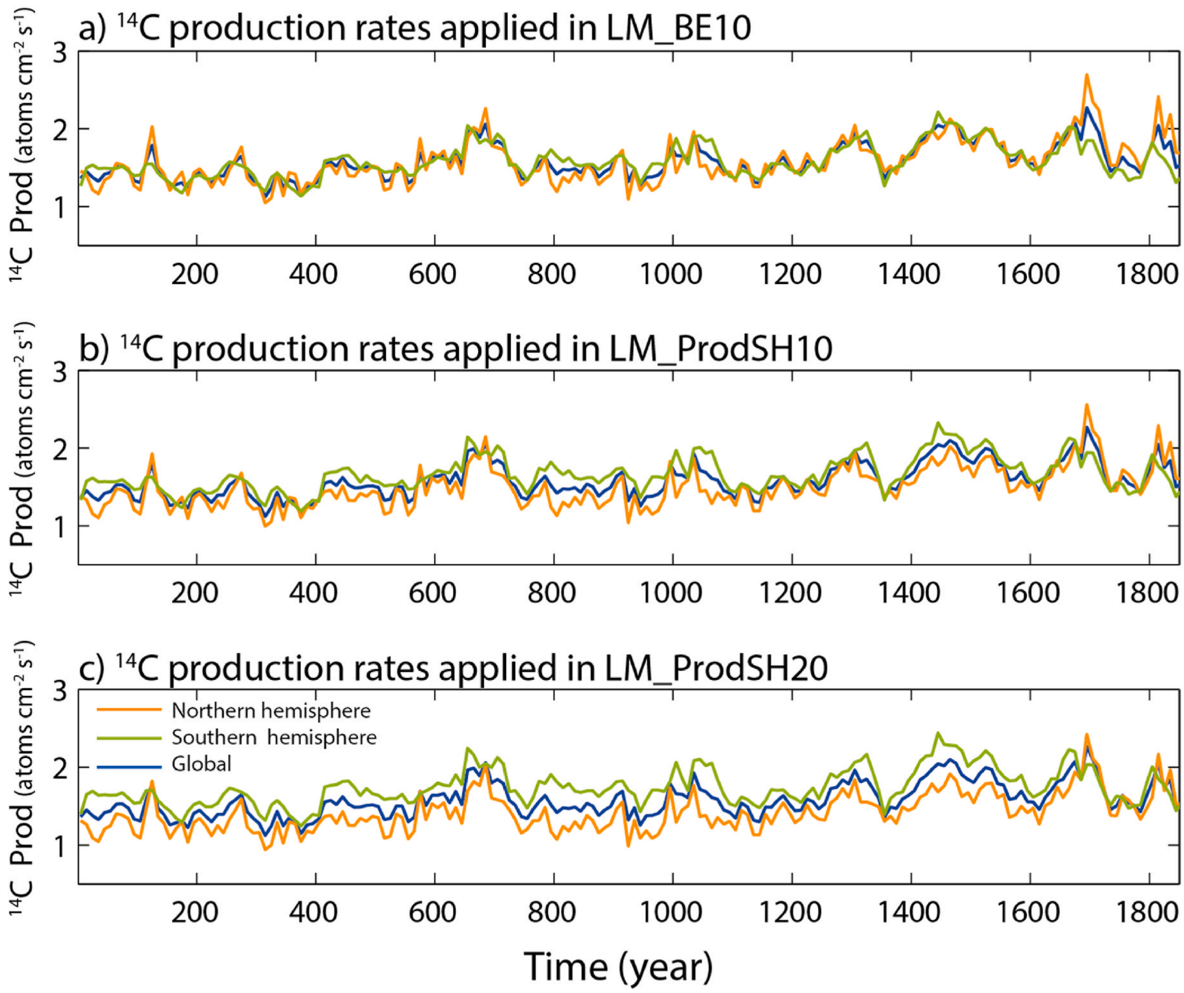

Fig. 2. ^{14}C production rate (atoms cm^{-2} s^{-1}) derived from ^{10}Be measurements for the northern hemisphere (orange), the southern hemisphere (light green) and the global mean (blue) a) with the same mean in the two hemispheres (used in LM_BE10) b) with a 10% higher production rate in the southern hemisphere (used in LM_ProdSH10) and c) with a 20% higher production rate in the southern hemisphere (used in LM_ProdSH20).

about 10 ‰ everywhere. This increase reduces the biases but the model values are still in general too low, in particular in the Antarctic Intermediate Waters and in the North Pacific at mid-depth (not shown).

In Ctrl1CE, the difference of atmospheric Δ^{14}C between the two hemispheres equals 1.3 ‰. This is much lower than the 4.5 ‰ mean difference over the period 1 CE–1850 CE between IntCal20 (Reimer et al., 2020) for the Northern Hemisphere and SHCal20 (Hogg et al., 2020) for the Southern Hemisphere. This difference can be due to several reasons. First, the diffusive atmospheric model applied in LOVECLIM for atmospheric Δ^{14}C is a very crude approximation of the real atmospheric transport. Second, the impact of oceanic circulation or atmosphere-ocean exchange on the interhemispheric differences could be underestimated in the model, for example because the SHWW tend to be too weak in LOVECLIM (Goosse et al., 2010). Third, SHCal20 and IntCal20 might not accurately represent the mean atmospheric Δ^{14}C over the whole hemisphere as a large fraction of the ^{14}C data is coming from mid and high latitudes and observations in the tropics are scarce. In particular, SHCal20 is dominated by mid-latitudes observations, especially from New Zealand. Analytic inaccuracies in ^{14}C measurements might also play a small role for some specific time periods (Hogg et al., 2020). For instance, Rodgers et al. (2011) compared the difference between IntCal and SHCal to the difference between the midlatitudes in their model results instead of the simulated Δ^{14}C averaged over each hemisphere. Based on their modelling results, the difference between those two estimates of the interhemispheric gradient could be higher than 1‰. The simple atmospheric model used here does not allow for a deeper understanding of the origin of the differences between our results and IntCal20 and SHCal20, and this is also not the goal here. We could have tuned the diffusion coefficients in the atmospheric model to get values closer to the difference between IntCal20 and SHCal20 but it would have likely been just a way to mask other problems. We thus prefer to keep the coefficient based on the literature but, for plotting purposes, we will multiply the simulated interhemispheric difference by a factor of 3.5 so that it roughly matches the observations. This methodology allows us to quantitatively compare our different experiments to each other but, even though it does not affect the timing of the changes for the model data comparison, the magnitude of the difference with data should be interpreted bearing for this scaling factor in mind.

3. Results of the idealized experiments

The formation of polynyas in the Weddell Sea has only a marginal effect on atmospheric Δ^{14}C, with a decrease of 3‰ at the end of the experiment Poly compared to Ctrl1CE and a change of less than 1‰ in Poly10 (Fig. 4a). Because of the stronger ventilation in the Southern Ocean, oceanic Δ^{14}C increases at depth by up to 5‰ in Poly, which slightly reduces the model biases (not shown). The adjustment is very slow, taking several centuries. Consequently, while the intermittency of the polynya formation at decadal time scale in Poly10 has, by construction, a strong impact on some variables like the sea ice

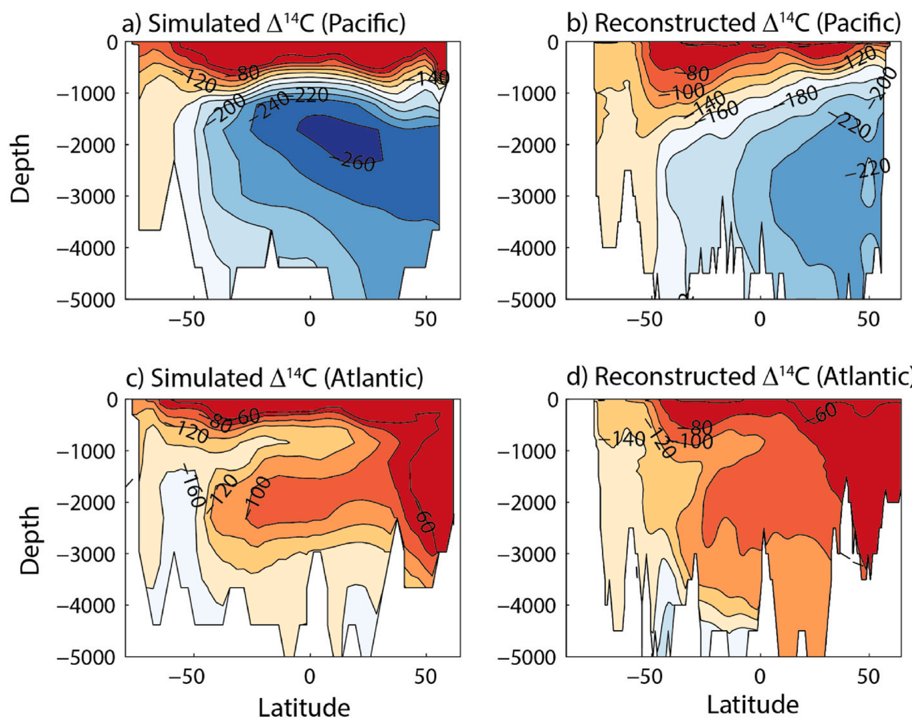

Fig. 3. $\Delta^{14}C$ for oceanic section at 150°W (Pacific) and 30°W (Atlantic) averaged over the years 1700–1800 CE in the simulation LM_Be10 (a and c) and for pre-industrial conditions and as estimated by GLODAP (b and d, Key et al., 2004). Contour interval is 20 ‰.

concentration, no decadal scale fluctuation is visible on the atmospheric $\Delta^{14}C$. Furthermore, the impact on the interhemispheric gradient is negligible for both experiments (Fig. 4b).

Changes in deep water formation in the North Atlantic had a large impact on the atmospheric $\Delta^{14}C$ on millennial time scales. For example, large disruptions of the Atlantic meridional overturning circulation (AMOC) during the deglaciation have induced changes in the atmospheric $\Delta^{14}C$ that might have exceeded 30 ‰ (e.g., Muscheler et al., 2000; Meissner et al., 2003; Butzin et al., 2005; Meissner, 2007; Köhler et al., 2006; Reimer et al., 2020). In FreshAtl, the maximum of the overturning streamfunction in the North Atlantic, is reduced by nearly 30 %, a change larger than those estimated for the past two millennia (e.g. Rahmstorf et al., 2015; Thornalley et al., 2018). This decrease in overturning leads to an increase in the atmospheric $\Delta^{14}C$ of 9 ‰ after 1000 years, i.e. a variation that is much smaller than during the deglaciation but in line with the smaller reduction of the overturning circulation in this sensitivity experiment. The impact of the perturbation is weaker in FreshSO, the maximum of the overturning streamfunction in the Southern Ocean close to Antarctica being reduced by 20 % and the atmospheric $\Delta^{14}C$ increasing by 5 ‰. As in Poly, the response is very slow in FreshAtl and FreshSO and the impact on the hemispheric gradients is also very small.

The effect of an increase in wind speed and wind stress over the Southern Ocean is much faster and stronger, with a decrease of atmospheric $\Delta^{14}C$ by nearly 10‰ and an increase of the interhemispheric difference by 2‰ in less than 100 years in Windstep. Stronger winds induce stronger upwelling of circumpolar deep waters and lead to a decrease of the $\Delta^{14}C$ at the surface of the Southern Ocean. The higher wind speed also leads to larger fluxes at the ocean-atmosphere interface and thus a smaller disequilibrium between the atmosphere and the ocean. Both processes contribute to a local decrease in atmospheric $\Delta^{14}C$ which quickly propagates to the whole atmosphere and then back to the ocean that displays a global decrease of surface $\Delta^{14}C$ (Fig. 5). However, as the input at surface in the Southern Ocean of ^{14}C depleted deep water is higher than in Ctrl1CE, the interhemispheric gradient of atmospheric $\Delta^{14}C$ also stays larger in Windstep. Because of this lower $\Delta^{14}C$ at ocean surface, the deep water masses formed in the North Atlantic have a lower $\Delta^{14}C$ content. The signal is weaker for Antarctic Bottom Water because of a compensation effect between lower surfaces values and higher ventilation rates in the Southern Ocean. At the same time, the higher oceanic ventilation increases oceanic $\Delta^{14}C$ at intermediate depths, with increases larger than 9‰ in the Pacific (Fig. 5).

In summary, our sensitivity experiments have shown that, although a change in deep water formation in the ocean in both hemispheres has an influence on atmospheric $\Delta^{14}C$, this requires changes in the oceanic circulation that are larger than these estimated for the past millennia. It takes also several centuries to observe the impact of those circulation changes, meaning that they could only have an influence on variations at multicentennial and longer timescales. Consequently, for reasonable changes in the ocean circulation compatible with estimates for the past two millennia, the main source of variability of atmospheric $\Delta^{14}C$ and in particular of its interhemispheric gradient, is likely due to changes in SHWW, justifying the choice of the sensitivity experiments discussed in section 4. This is in line with previous studies, in particular with Galbraith et al. (2011) who also analyzed the variability of $\Delta^{14}C$ associated with circulation changes, in their case in a control simulation performed with a coupled general circulation model. They also find that the impact of polynya formation on atmospheric $\Delta^{14}C$ is weak, partly because of the small surface covered by these polynyas. The simulated $\Delta^{14}C$ variations are instead dominated by those of the winds in the Southern Ocean because of the upwelling of water with a low ^{14}C content and the efficient air-sea exchanges due to the strong winds (Galbraith et al., 2011; Rodgers et al., 2011).

4. Simulations over the past two millennia

The standard simulation covering the past two millennia (LM_BE10) reproduces the observed atmospheric $\Delta^{14}C$ very well, leading to correlations with observations higher than 0.9 in both hemispheres (Fig. 6). These high correlations confirm that changes in atmospheric $\Delta^{14}C$ are dominantly driven by changes in the ^{14}C production rates. The variability of winds and oceanic circulation at decadal and longer timescales

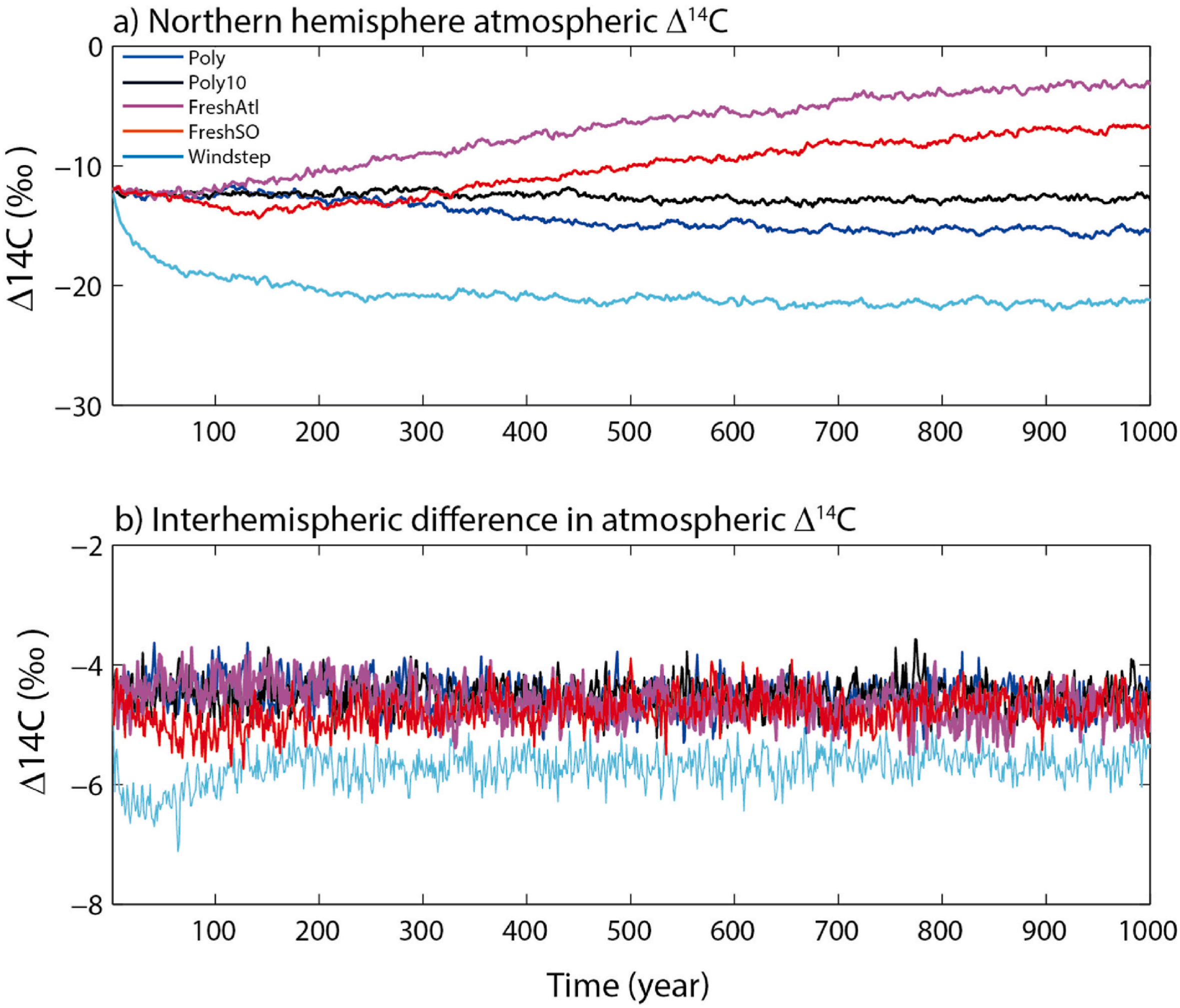

Fig. 4. a) Evolution of the northern hemisphere atmospheric $\Delta^{14}C$ and b) the interhemispheric difference (southern hemisphere mean minus northern hemisphere mean atmospheric $\Delta^{14}C$) in the 5 sensitivity experiments: Poly (blue), Poly10 (black), FreshAtl (magenta), FreshSO (red) and Windstep (cyan).

is very weak in LM_BE10 and our results show that a higher simulated variability is not required to simulate adequately hemispheric mean atmospheric $\Delta^{14}C$ changes over that period. It also indicates that the production rates deduced from ^{10}Be are consistent with measurements of $\Delta^{14}C$, providing a strong and independent validation. Nevertheless, LM_BE10 displays too low atmospheric $\Delta^{14}C$ around 400 CE compared to observations. The low production rate for this period derived from ^{10}Be observations (Fig. 2) leads to a decreasing trend in atmospheric $\Delta^{14}C$ that is larger than the observed one. Another disagreement between LM_BE10 and observations occurs between 1700 and 1850 CE, in particular in the southern hemisphere. This bias could indicate an overestimation in the production rate derived from ^{10}Be at that time or, alternatively, changes in the oceanic circulation that are not well represented by the model and would contribute to lower the atmospheric $\Delta^{14}C$.

Despite higher mean ^{14}C production rates in the southern than in the northern hemisphere in LM_ProdSH10 and LM_ProdSH20, the simulated hemispheric mean atmospheric $\Delta^{14}C$ remains so close to the values obtained in LM_BE10 that it is difficult to see any difference between them on Fig. 6. This indicates that the mixing between the two hemispheres is fast enough to compensate for the differences in hemispheric ^{14}C production rates. However, as expected, the interhemispheric difference in atmospheric $\Delta^{14}C$ is smaller in LM_ProdSH10 and LM_ProdSH20 than in LM_BE10 because the production in the southern hemisphere is larger in these experiments. The response appears relatively straightforward in LOVECLIM, with the curves in LM_ProdSH10 and LM_ProdSH20 simply shifted compared to LM_BE10.

Nevertheless, this larger production rate in the southern hemisphere in LM_ProdSH10 and LM_ProdSH20 is not able to compensate for the Southern Ocean source of depleted ^{14}C associated with the upwelling of deep water masses and the atmospheric $\Delta^{14}C$ remains lower in the southern hemisphere in all the experiments. In Ctrll1CE, the flux of ^{14}C from the atmosphere to the ocean in the southern hemisphere amounts to 234 molC $year^{-1}$ while it is of 156 molC $year^{-1}$ in the northern hemisphere. To achieve the same balance in both hemispheres in our model, the southern hemisphere would need to receive about 60% of the total production (234/390) and the northern hemisphere 40% (156/390). If this is not the case, a transport must occur from one hemisphere to the other, controlling the hemispheric gradient. While this is a rough calculation that does not include the contribution of continental surfaces, the estimate is consistent with a sensitivity test: to have similar $\Delta^{14}C$ in both hemispheres, about 65% of the production rate would be required in the southern hemisphere in LOVECLIM (not shown). Results from modelling of cosmogenic radionuclide production over the past 100,000 years (Panovska et al., 2023) never show hemispherical differences in production rates reaching this repartition of 60/40, explaining why in LM_ProdSH10 and LM_ProdSH20 the atmospheric $\Delta^{14}C$ is still lower in the southern hemisphere, in agreement with observations.

The amplitude of the fluctuations in interhemispheric ^{14}C gradient is much smaller in LM_BE10, LM_ProdSH10 and LM_ProdSH20 than the difference between SHCal20 and IntCal20, except after 1700 when the

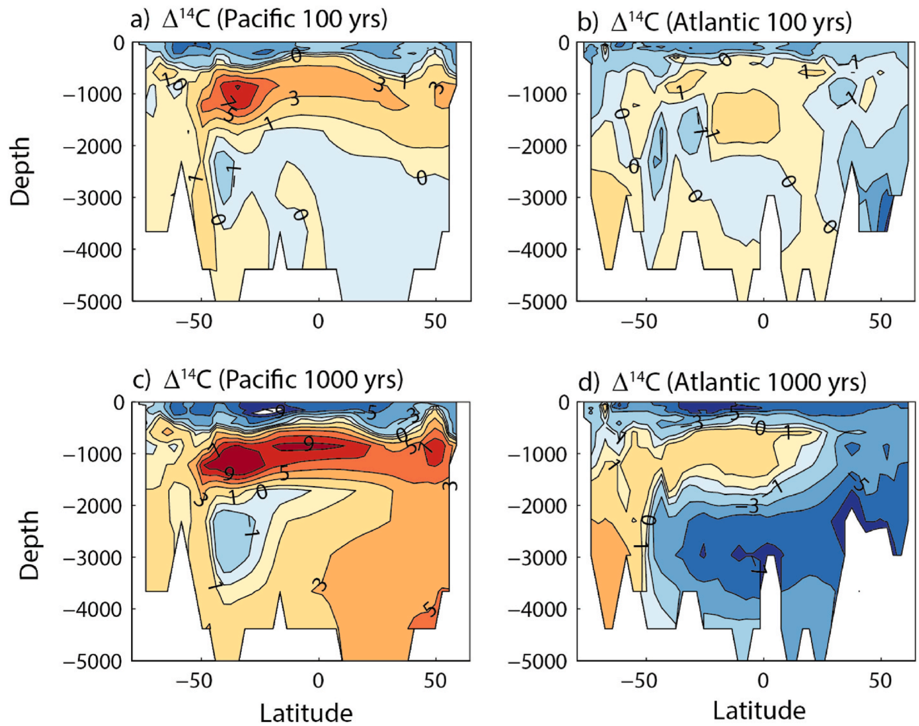

Fig. 5. Difference in Δ^{14}C for oceanic section at 150W (Pacific) (a and c) and 30W (Atlantic) (b and d) averaged over the years 1–100 (a and b) and 900–1000 (c and d) after the beginning of the wind perturbation in Windstep compared to the Ctrl1CE. Contour interval is 2 ‰ between −9‰ and 9‰ with an additional contour at 0‰.

simulated values strongly decrease in response to higher ^{14}C production in the northern hemisphere (Fig. 2). Overall, the correlation between simulated hemispheric differences in atmospheric Δ^{14}C and the difference between SHCal20 and IntCal20 is very close to zero. This indicates that, in our experiments, the difference in atmospheric ^{14}C production rate could not explain the observed interhemispheric differences in atmospheric Δ^{14}C.

When a wind perturbation proportional to the SAM index is applied, the mean atmospheric Δ^{14}C is impacted in both hemispheres by up to 5 ‰, with an increase in atmospheric Δ^{14}C when the SAM index decreases (Fig. 7). None of the three simulations (LM_SAM_Dat2018, LM_SAM_Dal2021 and LM_SAM_Kg2023) is clearly in better agreement with observations than the others but, for the period 1300–1700 CE, the observed interhemispheric gradient is within the range of the 3 simulations. However, the increase in the interhemispheric gradient at the beginning of the 18th century (i.e. more negative values in Fig. 7) is too strong in the three experiments. This is a period of increasing SAM index in the reconstructions, which is consistent with this increase, but the trend is larger than in the observations because the applied ^{14}C production rates (Fig. 2) becomes lower in the southern hemisphere than in the northern hemisphere at that time (and thus an increase in the interhemispheric gradient is already observed in LM_Be10, see Fig. 6). Over the period 1300–1800 CE, the correlation between simulated and observed interhemispheric gradient reaches 0.30, 0.31, and 0.12 for LM_SAM_Dat2018, LM_SAM_Dal2021 and LM_SAM_Kg2023, respectively. This is still relatively modest but much higher than for LM_Be10 (correlation of 0.01 over this period) and is consistent with the correlation between the SAM indices and the observed interhemispheric gradient (see Fig. 1 b) which equals 0.44, 0.41, and 0.22 for the period 1300–1800 for the reconstructions of Dätwyler et al. (2018), Dalaiden et al. (2021) and King et al. (2023), respectively. If we take the difference between the three wind perturbation experiments and LM_Be10 to remove the contribution of the interhemispheric difference in production rate, the correlation increases to 0.43, 0.41 and 0.19, showing the direct and relatively linear link between the applied SAM variations and interhemispheric gradient in atmospheric Δ^{14}C in our experiments. More specifically, the three reconstructions display relatively high values of the SAM index between 1200 and 1350 CE, a decrease around the 15th century before a positive trend and higher values. This implies that in LM_SAM_Dat2018, LM_SAM_Dal2021 and LM_SAM_Kg2023 the lowest value of the interhemispheric gradient occurs in the 14th century with a peak at around 1500 in good agreement with the observations. Before 1300 CE, the model-data agreement is much lower but this could be due to the lower skill of the SAM reconstructions as the number of available proxies is decreasing the further we go back, as highlighted by the large differences between the 3 reconstructions at that time.

5. Conclusions

Our simulations have confirmed the hypothesis that the global and hemispheric mean variations in atmospheric Δ^{14}C over the past two millennia are mainly controlled by changes in the ^{14}C production rate. Modulations by the atmospheric and oceanic circulation are possible but their contribution is at least an order of magnitude smaller. Our results also indicate a very good agreement between observed and simulated atmospheric Δ^{14}C when the model is driven by production rates derived from ^{10}Be. This agreement indicates that the independent time series of those two cosmogenic isotopes are very consistent. Reconstructions of solar activity based on those series are therefore trustworthy and not strongly impacted by the uncertainties on these records or by atmospheric or oceanic circulations changes. Our simulations suggest that the ^{14}C production rate derived from the ^{10}Be is slightly too low around 400 CE and slightly too high between 1650 and 1800 CE. This bias may be due to factors affecting ^{10}Be deposition that are not well accounted for in the estimate of the production rate or to carbon-cycle effects on Δ^{14}C that are not adequately represented by our model. We could not determine here which one is responsible for the discrepancy but, as the atmospheric Δ^{14}C is mainly controlled by the production rate, biases in the model input for the production rate is a likely candidate.

LOVECLIM simulates lower atmospheric Δ^{14}C in the southern

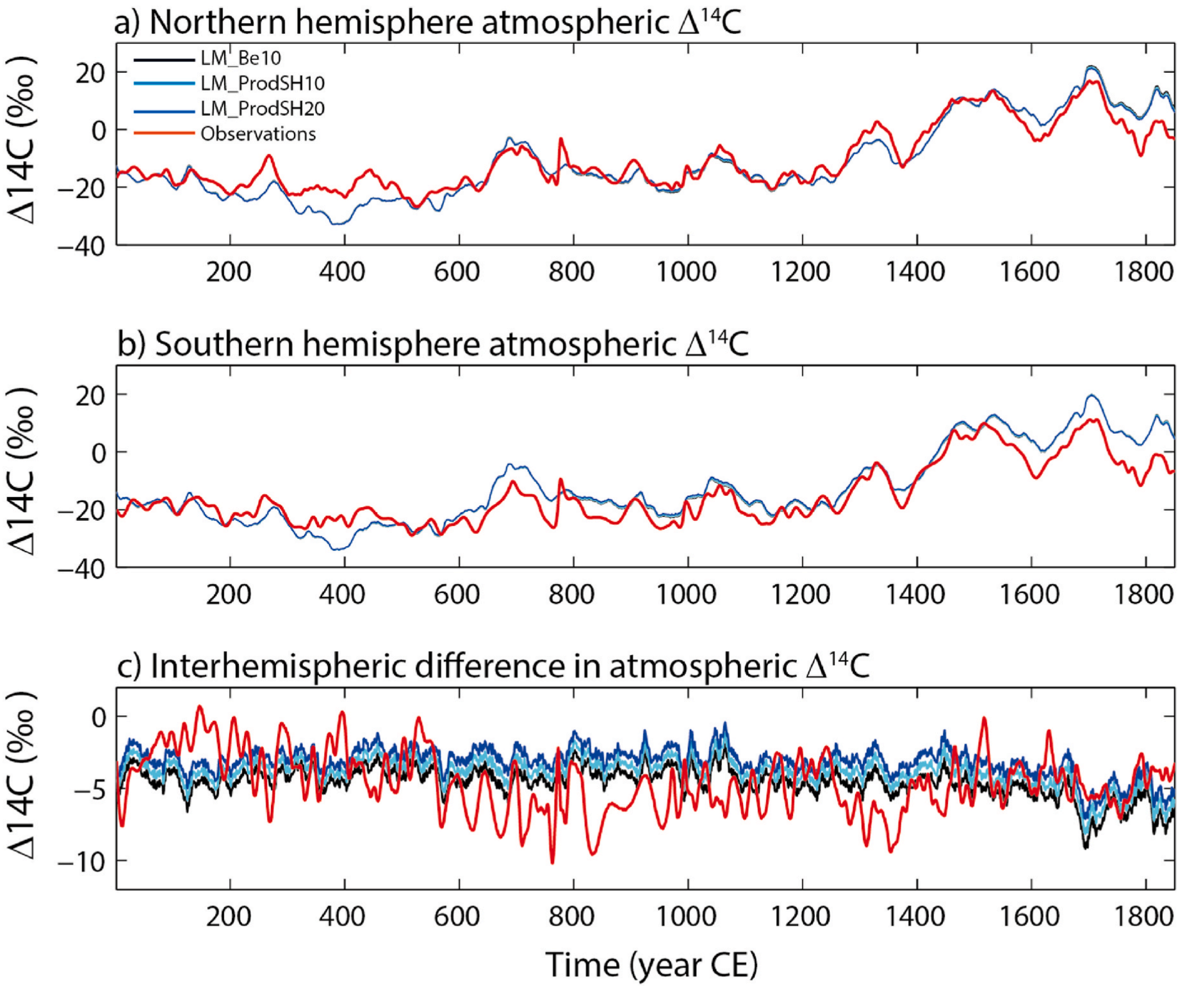

Fig. 6. a) Simulated atmospheric $\Delta^{14}C$ in the northern hemisphere in LM_Be10 (black) LM_ProdSH10 (cyan) and in LM_ProdSH20 (blue) and observed (red). b) Same for the southern hemisphere and c) Difference in atmospheric $\Delta^{14}C$ between the two hemispheres (southern hemisphere mean minus northern hemisphere mean) for the three simulations and observations. The simulated differences have been scaled by a factor 3.5 (see section 2c). The curves for the three simulations on panel a and b are so close to each other that it is hard to distinguish them on a plot.

hemisphere than in the northern hemisphere over the preindustrial common era, despite a generally higher ^{14}C production rate in the southern hemisphere due to asymmetries in the geomagnetic field. This lower atmospheric $\Delta^{14}C$ in the southern hemisphere is due to the dominant effect of upwelling of ^{14}C depleted deep-water masses induced by the strong SHWW (Rodgers et al., 2011). Nevertheless, the simulated interhemispheric difference in atmospheric $\Delta^{14}C$ is much lower than the difference between IntCal20 and SHCal20. There are some uncertainties to what extent IntCal20 and SHCal20 represent true hemispheric means (Reimer et al., 2020; Hogg et al., 2020) and thus provide an unbiased estimate of interhemispheric gradients. However, the model likely underestimates changes due to a coarse resolution and simplified process parameterizations, which could significantly influence the magnitude of the difference in atmospheric $\Delta^{14}C$ between the two hemispheres. In particular, the simulated winds are relatively weak over the Southern Ocean, potentially leading to too low atmosphere-ocean transfer of ^{14}C there. Furthermore, the meridional atmospheric transport of ^{14}C is crudely represented by diffusion in one single layer, which is obviously a very strong approximation. The sensitivity experiments performed here are internally consistent and can directly be compared to each other but any quantitative interpretation of our results and comparison with observations should be viewed within the framework of this difference with observations.

We find that changes in polynya formation in the Southern Ocean or in deep water formation in both hemispheres had likely only a small effect on atmospheric $\Delta^{14}C$ over the past two millennia, in agreement with Galbraith et al. (2011). By contrast, because of the strong effect of changes in Southern Ocean upwelling on atmospheric ^{14}C, the interhemispheric differences in atmospheric $\Delta^{14}C$ are very sensitive to variations in SHWW. When driven by changes in the SHWW proportional to three different reconstructions of the SAM index, the fluctuations in simulated interhemispheric differences in atmospheric $\Delta^{14}C$ are much larger than those resulting from changes in production rates in the two hemispheres, suggesting that the interhemispheric difference in production rates is not the main cause of the observed interhemispheric difference in $\Delta^{14}C$. However, we have to acknowledge that the uncertainties in both production rates and atmospheric $\Delta^{14}C$ might be too large to obtain a meaningful link between them, and that the model might have too large biases to reproduce the observed link trustworthily.

In response to perturbations in SHWW proportional to SAM index reconstructions, simulated and observed interhemispheric differences in atmospheric $\Delta^{14}C$ do not strictly follow each other but some clear common features are present after 1400 CE. These include relatively low values in the 15th century, and a peak in the 16th century followed by a decreasing trend. This indicates that, despite their differences, SAM reconstructions robustly represent some large centennial variations in the strength of westerly winds, even if the SAM evolution before 1400 CE is uncertain. This independent confirmation of the existence of large centennial variability in SHWW in the past further suggests that the inability of climate models to reproduce the variability in SAM

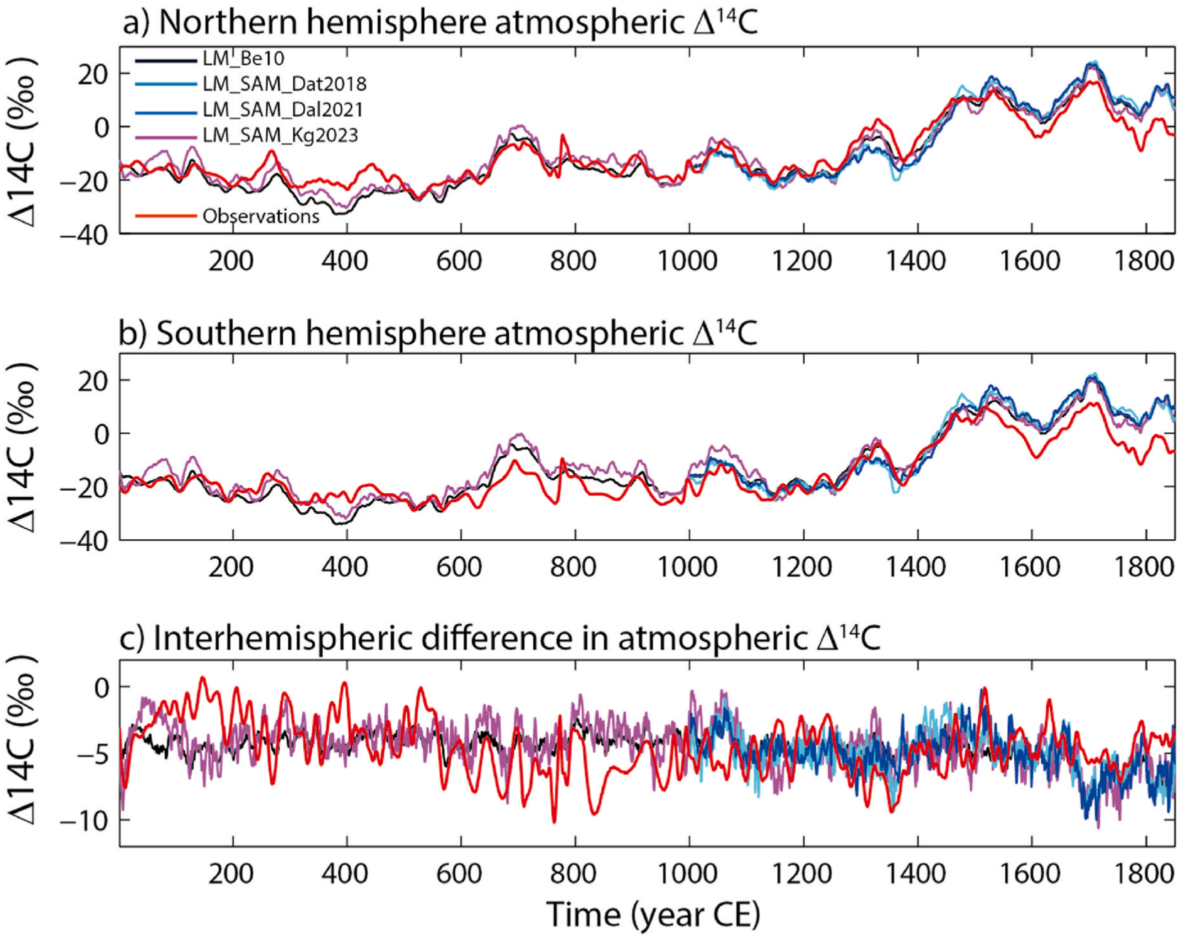

Fig. 7. a) Simulated atmospheric $\Delta^{14}C$ in the northern hemisphere for LM_Be10 (black) and in the simulation driven by changes in the winds proportional to reconstructions of the SAM index: LM_SAM_Dat2018 (cyan), LM_SAM_Dal2021(blue), LM_SAM_Kg2023 (magenta), and observed (red). b) Same for the southern hemisphere. c) Atmospheric $\Delta^{14}C$ difference between the two hemispheres (southern hemisphere mean minus northern hemisphere mean) for the four simulations and observations. The simulated difference has been scaled by a factor 3.5 to have the same mean as the observations (see section 2c).

reconstructions (Abram et al., 2014) is likely not due to uncertainties in these SAM reconstructions but is rather caused by some biases in the simulations. Finally, our results illustrate that $\Delta^{14}C$ is a powerful tool to infer oceanic and atmospheric circulation changes not only on multi-millennial timescales during the past glacial period or the deglaciation but also over the Holocene. In particular, combining observations of the interhemispheric $\Delta^{14}C$ gradient with other proxies of westerly winds, such as glacier length (Bakke et al., 2021; Charton et al., 2022), information from lake and ocean sediments cores (Lamy et al., 2010; Perren et al., 2020; Saunders et al., 2018) and fire activity (Fletcher et al., 2018), is a promising avenue to robustly reconstruct past changes in SAM.

CRediT authorship contribution statement

Hugues Goosse: Conceptualization, Methodology, Software, Validation, Investigation, Writing - original draft, Writing - review & editing, Visualization, Supervision. **Victor Brovkin:** Conceptualization, Writing - review & editing. **Katrin J. Meissner:** Conceptualization, Writing - review & editing. **Laurie Menviel:** Conceptualization, Writing - review & editing. **Anne Mouchet:** Conceptualization, Methodology, Software, Writing - review & editing. **Raimund Muscheler:** Conceptualization, Data curation, Formal analysis, Writing - review & editing. **Andreas Nilsson:** Conceptualization, Formal analysis, Data curation, Writing - review & editing.

Declaration of competing interest

The authors declare that they have no known competing financial interests or personal relationships that could have appeared to influence the work reported in this paper.

Data availability

Data will be made available on request.

Acknowledgements

Hugues Goosse is research director at the Fonds de la Recherche Scientifique (F.R.S.-FNRS). Anne Mouchet benefited from support from the F.R.S.-FNRS. This work was funded by the Belgian F.R.S.-FNRS. Victor Brovkin acknowledges support through the project PalMod, funded by the German Federal Ministry of Education and Research (BMBF). Katrin Meissner and Laurie Menviel acknowledge funding from the Australian Research Council (DP180100048, FT180100606, SR200100008). Raimund Muscheler acknowledges funding from the Swedish Research Council (DNR2013-8421, DNR2018-05469). Andreas Nilsson acknowledges funding from the Swedish Research Council (DNR2020-04813). Computational resources have been provided by the supercomputing facilities of the Université catholique de Louvain (CISM/UCLouvain) and the Consortium des Équipements de Calcul Intensif en Fédération Wallonie Bruxelles (CÉCI) funded by F.R.S.-FNRS under convention 2.5020.11 and by the Walloon Region. We would also want to thank the scientists that collected and shared their records and reconstructions, as without those, the present study would not have been possible.

References

Abram, N.J., Mulvaney, R., Vimeux, F., et al., 2014. Evolution of the southern annular Mode during the past millennium. Nat. Clim. Change 4, 564–569.

Bakke, J., Paasche, Ø., Schaefer, J., Timmermann, A., 2021. Long-term demise of sub-Antarctic glaciers modulated by the Southern Hemisphere Westerlies. Sci. Rep. 11, 8361.

Bard, E., Raisbeck, G.M., Yiou, F., Jouzel, J., 1997. Solar modulation of cosmogenic nuclide production over the last millennium: comparison between 14C and 10Be records. Earth Planet Sci. Lett. 150, 453–462.

Bauska, T.K., Baggenstos, D., Brook, et al., 2016. Carbon isotopes characterize rapid changes in atmospheric carbon dioxide during the last deglaciation. Proc. Natl. Acad. Sci. U.S.A. 113, 3465–3470.

Broecker, W., Andree, M., Bonani, G., et al., 1988. Preliminary estimates for the radiocarbon age of deep water in the glacial ocean. Paleoceanography 3 (6), 659–669.

Broecker, W.S., Virgilio, A., Peng, T.-H., 1991. Radiocarbon age of waters in the deep Atlantic revisited. Geophys. Res. Lett. 18, 1–3.

Brovkin, V., Ganopolski, A., Svirezhev, Y., 1997. A continuous climate vegetation classification for use in climate-biosphere studies. Ecol. Model. 101, 251–261.

Butzin, M., Prange, M., Lohmann, G., 2005. Radiocarbon simulations for the glacial ocean: the effects of wind stress, Southern Ocean sea ice and Heinrich events. Earth Planet Sci. Lett. 235, 45–61.

Capano, M., Miramont, C., Shindo, L., et al., 2020. Onset of the Younger Dryas recorded with ^{14}C at annual resolution in French subfossil trees. Radiocarbon 62 (4), 901–918.

Charton, J., Schimmelpfennig, I., Jomelli, V., et al., 2022. New cosmogenic constraints on late glacial and Holocene glacier fluctuations in the sub-antarctic Indian ocean (Kerguelen Islands, 49°S). Quat. Sci. Rev. 283, 107461.

Dalaiden, Q., Goosse, H., Rezsohazy, J., Thomas, E.R., 2021. Reconstructing atmospheric circulation and sea-ice extent in the West Antarctic over the past 200 years using data assimilation. Clim. Dynam. 57, 3479–3503.

Dätwyler, C., Neukom, R., Abram, N.J., et al., 2018. Teleconnection stationarity, variability and trends of the Southern Annular Mode (SAM) during the last millennium. Clim. Dynam. 51, 2321–2339.

Deleersnijder, E., Campin, J.-M., Delhez, E., 2001. The concept of age in marine modelling. I. Theory and preliminary model results. J. Mar. Syst. 28, 229–267.

Dinauer, A., Adolphi, F., Joos, F., 2020. Mysteriously high Δ^{14}C of the glacial atmosphere: influence of ^{14}C production and carbon cycle changes. Clim. Past 16 (4), 1159–1185.

England, M.H., Maier-Reimer, E., 2001. Using chemical tracers to assess ocean models. Rev. Geophys. 39, 29–70.

Fletcher, M.S., Benson, A., Bowman, D.M.J.S., et al., 2018. Centennial-scale trends in the Southern Annular Mode revealed by hemisphere-wide fire and hydroclimatic trends over the past 2400 years. Geology 46 (4), 363–366.

Galbraith, E.D., Kwonn, E.Y., Gnanadesikan, A., et al., 2011. Climate variability and radiocarbon in the CM2Mc Earth system model. J. Clim. 24, 4230–4254.

Ganopolski, A., Brovkin, V., 2017. Simulation of climate, ice sheets and CO2 evolution during the last four glacial cycles with an Earth system model of intermediate complexity. Clim. Past 13, 1695–1716.

Geller, L.S., Elkins, J.W., Lobert, J.M., et al., 1997. Tropospheric SF_6: observed latitudinal distribution and trends, derived emissions and interhemispheric exchange time. Geophys. Res. Lett. 24, 675–678.

Goosse, H., Fichefet, T., 1999. Importance of ice-ocean interactions for the global ocean circulation: a model study. J. Geophys. Res. 104, 23337–23355.

Goosse, H., Brovkin, V., Fichefet, T., et al., 2010. Description of the Earth system model of intermediate complexity LOVECLIM version 1.2. Geosci. Model Dev. (GMD) 3, 603–633.

Goosse, H., Barriat, P.-Y., Klein, F., 2022. Changes in atmospheric CO2 concentration over the past two millennia: contribution of climate variability, land-use and Southern Ocean dynamics. Clim. Dynam. 58, 2957–2979.

Hain, M.P., Sigman, D.M., Haug, G.H., 2014. Distinct roles of the Southern Ocean and North Atlantic in the deglacial atmospheric radiocarbon decline. Earth Planet Sci. Lett. 394, 98–208.

Heaton, T.J., Bard, E., Bronk Ramsey, C., et al., 2021. Radiocarbon: a key tracer for studying Earth's dynamo, climate system, carbon cycle, and Sun. Science 374, 6568.

Herbst, K., Muscheler, R., Heber, B., 2017. The new local interstellar spectra and their influence on the production rates of the cosmogenic radionuclides 10Be and 14C. J. Geophys. Res.: Space Phys. 122 (1), 23–34.

Hogg, A.G., Heaton, T.J., Hua, Q., et al., 2020. SHCal20 southern hemisphere calibration, 0–55,000 Years cal BP. Radiocarbon 62 (4), 759–778.

Jahn, A., Lindsay, K., Giraud, X., et al., 2015. Carbon isotopes in the ocean model of the community earth system model (CESM1). Geosci. Model Dev. (GMD) 8 (8), 2419–2434.

Jackson, L.C., Alastrué de Asenjo, E., Bellomo, K., et al., 2023. Understanding AMOC stability: the North Atlantic hosing model Intercomparison project. Geosci. Model Dev. (GMD) 16, 1975–1995.

Jungclaus, J.H., Bard, E., Baroni, M., et al., 2017. The PMIP4 simulations of the last millennium (PMIP past1000). Geosci. Model Dev. (GMD) 10, 4005–4033.

Key, R.M., Kozyr, A., Sabine, C.L., et al., 2004. A global ocean carbon climatology: results from global data analysis project (GLODAP). Global Biogeochem. Cycles 18, GB4031.

King, J.K., Anchukaitis, J., Allen, K., Vance, T., Hessl, A., 2023. Trends and variability in the southern annular Mode over the common era. Nat. Commun. 14, 2324.

Köhler, P., Fischer, H., Munhoven, G., Zeebe, R.E., 2005. Quantitative interpretation of atmospheric carbon records over the last glacial termination. Global Biogeochem. Cycles 19, 1–24.

Köhler, P., Muscheler, R., Fischer, H., 2006. A model-based interpretation of low frequency changes in the carbon cycle during the last 120,000 years and its implications for the reconstruction of atmospheric Δ 14C. G-cubed 7, Q11N06.

Köhler, P., Knorr, G., Bard, E., 2014. Permafrost thawing as a possible source of abrupt carbon release at the onset of the Bølling/Allerød. Nat. Commun. 5, 5520.

Köhler, P., Adolphi, F., Butzin, M., Muscheler, R., 2022. Toward reconciling radiocarbon production rates with carbon cycle changes of the last 55,000 years. Paleoceanogr. Paleoclimatol. 37, e2021PA004314.

Kovaltsov, G.A., Mishev, A., Usoskin, I.G., 2012. A new model of cosmogenic production of radiocarbon ^{14}C in the atmosphere. Earth Plan. Sc. Lett. 337–338, 114–120.

Laepple, T., Huybers, P., 2014. Ocean surface temperature variability: large model–data differences at decadal and longer periods. Proc. Nat. Acad. Sciences 111 (47), 16682–16687.

Lal, D., Peters, B., 1967. Cosmic ray produced radioactivity on the earth. In: Sittle, K. (Ed.), Kosmische Strahlung II/Cosmic Rays II Handbuch der Physik/Encyclopedia of Physics, 9. Springer, Berlin, pp. 551–612.

Lamy, F., Kilian, R., Arz, H.W., et al., 2010. Holocene changes in the position and intensity of the southern westerly wind belt. Nat. Geosci. 3, 695–699.

Levin, I., Kromer, B., Wagenbach, D., Münnich, K.O., 1987. Carbon isotope measurements of atmospheric CO_2 at a coastal station in Antarctica. Tellus B 39 (1–2), 89–95.

Masarik, J., Beer, J., 1999. Simulation of particle fluxes and cosmogenic nuclide production in the Earth's atmosphere. J. Geophys. Res. 104 (D10), 12099–12111.

Matsumoto, K., Sarmiento, J.L., Key, R.M., et al., 2004. Evaluation of ocean carbon cycle models with data-based metrics. Geophys. Res. Lett. 31, L07303.

Meissner, K.J., Schmittner, A., Weaver, A.J., Adkins, J.F., 2003. Ventilation of the North Atlantic ocean during the last glacial maximum: a comparison between simulated and observed radiocarbon ages. Paleoceanography 18 (2), 1023.

Meissner, K.J., 2007. Younger Dryas: a data to model comparison to constrain the strength of the overturning circulation. Geophys. Res. Lett. 34, L21705.

Menviel, L., Yu, J., Joos, F., Mouchet, A., Meissner, K.J., England, M.H., 2017. Poorly ventilated deep ocean at the Last Glacial Maximum inferred from carbon isotopes: a data-model comparison study. Paleoceanography 32 (1), 2–17.

Menviel, L., Spence, P., Yu, J., Chamberlain, M.A., Matear, R.J., Meissner, K.J., England, M.H., 2018. Southern Hemisphere westerlies as a driver of the early deglacial atmospheric CO_2 rise. Nat. Commun. 9, 2503.

Mouchet, A., 2011. A 3D model of ocean biogeochemical cycles and ocean ventilation studies. PhD. Thesis. Université de Liège, p. 222p.

Muscheler, R., Beer, J., Wagner, G., Finkel, R.C., 2000. Changes in deep-water formation during the Younger Dryas event inferred from ^{10}Be and ^{14}C records. Nature 408 (6812), 567–570.

Muscheler, R., Joos, F., Beer, J., Mueller, S.A., Vonmoos, M., Snowball, I., 2007. Solar activity during the last 1000 yr inferred from radionuclide records. Quat. Sci. Rev. 26, 82–87.

Mouchet, A., François, L.M., 1996. Sensitivity of a global oceanic carbon cycle model to the circulation and the fate of organic matter: preliminary results. Phys. Chem. Earth 21, 511–516.

Muscheler, R., Adolphi, F., Herbst, K., Nilsson, A., 2016. The revised sunspot record in comparison to cosmogenic radionuclide-based solar activity reconstructions. Sol. Phys. 291, 3025–3043.

Orr, J.C., Najjar, R.G., Aumont, O., et al., 2017. Biogeochemical protocols and diagnostics for the CMIP6 ocean model Intercomparison project (OMIP). Geosci. Model Dev. (GMD) 10 (6), 2169–2199.

Opsteegh, J.D., Haarsma, R.J., Selten, F.M., Kattenberg, A., 1998. ECBilt: a dynamic alternative to mixed boundary conditions in ocean models. Tellus 50A 348–367.

Panovska, S., Poluianov, S., Gao, J., Korte, M., Mishev, A., Shprits, Y.Y., Usoskin, I., 2023. Effects of global geomagnetic field variations over the past 100,000 Years on cosmogenic radionuclide production rates in the earth's atmosphere. J. Geophys. Res.: Space Phys. 128, e2022JA031158.

Perren, B.B., Hodgson, D.A., Roberts, S.J., et al., 2020. Southward migration of the Southern Hemisphere westerly winds corresponds with warming climate over centennial timescales. Commun Earth Environ 1, 58. https://doi.org/10.1038/s43247-020-00059-6.

Poluianov, S.V., Kovaltsov, G.A., Mishev, A.L., Usoskin, I.G., 2016. Production of cosmogenic isotopes 7Be, 10Be, 14C, 22Na, and 36Cl in the atmosphere: altitudinal profiles of yield functions. J. Geophys. Res.: Atmospheres 121 (13), 8125–8136.

Pookkandy, B., Graven, H., Martin, A., 2023. Contemporary oceanic radiocarbon response to ocean circulation changes. Clim. Dynam. 61, 3223–3235.

Rahmstorf, S., Box, J.E., Feulner, G., et al., 2015. Exceptional twentieth-century slowdown in Atlantic Ocean overturning circulation. Nat. Clim. Change 5, 475–480, 2015.

Reimer, P.J., Austin, W.E.N., Bard, E., et al., 2020. The IntCal20 northern hemisphere radiocarbon age calibration curve (0–55 cal kBP). Radiocarbon 62 (4), 725–757.

Rodgers, K.B., Mikaloff-Fletcher, S.E., Bianchi, D., et al., 2011. Interhemispheric gradient of atmospheric radiocarbon reveals natural variability of Southern Ocean winds. Clim. Past 7, 1123–1138.

Roth, R., Joos, F., 2013. A reconstruction of radiocarbon production and total solar irradiance from the Holocene ^{14}C and CO_2 records: implications of data and model uncertainties. Clim. Past 9, 1879–1909, 2013.

Saunders, K.M., Roberts, S.J., Perren, B., 2018. Holocene dynamics of the Southern Hemisphere westerly winds and possible links to CO2 outgassing. Nat. Geosci. 11, 650–655.

Schaefer, J., 2022. South Pole Ice Core 10Be CEU.S. Antarctic Program (USAP) Data Center.

Skinner, L.C., Primeau, F., Freeman, E., et al., 2017. Radiocarbon constraints on the glacial ocean circulation and its impact on atmospheric CO_2. Nat. Commun. 8, 16010.

Skinner, L.C., Primeau, F., Jeltsch-Thömmes, A., et al., 2023. Rejuvenating the ocean: mean ocean radiocarbon, CO_2 release, and radiocarbon budget closure across the last deglaciation. Clim. Past 19, 2177–2202.

Skinner, L.C., Bard, E., 2022. Radiocarbon as a dating tool and tracer in paleoceanography. Rev. Geophys. 60, e2020RG000720.

Stuiver, M., Polach, H.A., 1977. Discussion: reporting of ^{14}C data. Radiocarbon 19, 355–363.

Swart, N.C., Martin, T., Beadling, R., et al., 2023. The Southern Ocean Freshwater Input from Antarctica (SOFIA) Initiative: scientific objectives and experimental design. Geos. Mod. Dev. 16, 7289–7309.

Thornalley, D.J.R., Oppo, D.W., Ortega, P., et al., 2018. Anomalously weak Labrador Sea convection and Atlantic overturning during the past 150 years. Nature 556, 227–230.

Toggweiler, J.R., Dixon, K., Bryan, K., 1989. Simulations of radiocarbon in a coarse-resolution world ocean model, I,Ste ady state prebomb distributions. J. Geophys. Res. 94, 8217–8242.

Tschumi, T., Joos, F., Gehlen, M., Heinze, C., 2011. Deep ocean ventilation, carbon isotopes, marine sedimentation and the deglacial CO2 rise. Clim. Past 7, 771–800.

Winski, D.A., Fudge, T.J., Ferris, D.G., et al., 2019. The SP19 chronology for the South Pole Ice Core – Part 1: volcanic matching and annual layer counting. Clim. Past 15, 1793–1808.

Zheng, M., Adolphi, F., Paleari, C., et al., 2023. Solar, atmospheric, and volcanic impacts on 10Be depositions in Greenland and Antarctica during the last 100 years. J. Geophys. Res.: Atmospheres 128, e2022JD038392.

Zheng, M., Liu, H., Sylvaine, F., Adolphi, F., Lu, Z., Lohmann, U., in prep. Sensitive Studies of Atmospheric Transport Models in Simulating Be10 Depositions in Polar Regions Using GEOS-Chem and ECHAM6.3-HAM2.3 Models: Implication for Paleo-Solar and Paleo-Geomagnetic Reconstructions..